



HAL
open science

Contribution of meandering rivers to natural carbon fluxes: Evidence from the Ucayali River, Peruvian Amazonia

Romain Walcker, Dov Corenblit, Frédéric Julien, Jean-Michel Martinez, Johannes Steiger

► To cite this version:

Romain Walcker, Dov Corenblit, Frédéric Julien, Jean-Michel Martinez, Johannes Steiger. Contribution of meandering rivers to natural carbon fluxes: Evidence from the Ucayali River, Peruvian Amazonia. *Science of the Total Environment*, 2021, 776, pp.146056. 10.1016/j.scitotenv.2021.146056 . hal-03162177

HAL Id: hal-03162177

<https://uca.hal.science/hal-03162177v1>

Submitted on 8 Mar 2021

HAL is a multi-disciplinary open access archive for the deposit and dissemination of scientific research documents, whether they are published or not. The documents may come from teaching and research institutions in France or abroad, or from public or private research centers.

L'archive ouverte pluridisciplinaire **HAL**, est destinée au dépôt et à la diffusion de documents scientifiques de niveau recherche, publiés ou non, émanant des établissements d'enseignement et de recherche français ou étrangers, des laboratoires publics ou privés.

1 **Contribution of meandering rivers to natural carbon fluxes: evidence from the Ucayali**
2 **River, Peruvian Amazonia**

3 Romain Walcker¹, Dov Corenblit², Frédéric Julien¹, Jean-Michel Martinez³, Johannes Steiger²

4 ¹ Laboratoire Ecologie Fonctionnelle et Environnement, Université de Toulouse, CNRS,
5 Toulouse, France.

6 ² Université Clermont Auvergne, CNRS, GEOLAB, 63000 Clermont-Ferrand, France

7 ³ GET, Institut de Recherche pour le Développement, CNRS, Toulouse, France.

8 ***Corresponding author:**

9 Romain Walcker, Porte 336, Bât. 4R1, Université de Toulouse, 118 route de Narbonne 31062,
10 Toulouse, France.

11 Phone: +33-(0)5-61-55-89-27.

12 Fax: +33-(0)5-61-55-89-01.

13 E-mail: romain.walcker@univ-tlse3.fr

14 **Journal:** *Science of the Total Environment*

15 **Paper type:** Full papers

16 **Keywords:** Amazon; carbon; floodplain; forest age; meandering river; remote sensing;

17 **Contribution of meandering rivers to natural carbon fluxes: evidence from the Ucayali**
18 **River, Peruvian Amazonia**

19 **1. Abstract**

20 Better understanding the fate of the atmospheric carbon (C) captured by plant photosynthesis
21 is essential to improve natural C flux modelling. Soils are considered as the major terrestrial
22 bioreactor and repository of plant C, whereas channel networks of floodplain rivers collect and
23 transport, throughout the aquatic continuum, a significant part of plant primary production until
24 its export through outgassing or sequestration in marine sediments. Here, we show that river
25 meandering in forested floodplains is a crucial and widely overlooked Earth surface process
26 promoting C fluxes from the atmosphere to the aquatic continuum, via the floodplain
27 vegetation. Over a recent period of 35 years (1984-2019), we quantified those C fluxes in one
28 of the most active meandering rivers on Earth, the Ucayali River, Peru, South America. We
29 used map time series combined with above-ground forest C data to derive the amount of C that
30 is annually captured by the growing floodplain vegetation within the active meander belt, as
31 well as exported to the aquatic continuum by lateral channel erosion. We found that the annual
32 building and erosion of forested floodplain areas was nearly balanced over time with
33 $19.0 \pm 7.7 \times 10^3 \text{ ha}^{-1} \text{ yr}^{-1}$ and $19.8 \pm 6.7 \times 10^3 \text{ ha}^{-1} \text{ yr}^{-1}$, respectively. While growing forests within
34 the active meander belt annually captured $0.01 \pm 0.05 \times 10^6 \text{ Mg C yr}^{-1}$, lateral channel erosion
35 provided the nearly 100-fold amount of C to the river channel and its streamflow, i.e.
36 $0.9 \pm 0.4 \times 10^6 \text{ Mg C yr}^{-1}$. Our findings revealed that the migration of the Ucayali River channel
37 provided nearly 10-times more lignified C per unit area to the aquatic continuum (44.7 ± 21.4
38 $\text{Mg C ha}^{-1} \text{ yr}^{-1}$) than non-meandering central Amazonian floodplains do. Together, these
39 findings point to the importance of quantifying the overall contribution of meandering rivers to
40 natural C fluxes worldwide.

41 **2. Introduction**

42 Floodplains are areas of high primary production which provide fresh autochthonous carbon
43 (C) to river waters through litterfall, plant and micro-organism respiration (Abril *et al.*, 2014).
44 Levels of plant production in floodplains and the extent of the floodplain area can therefore
45 considerably modulate the overall C quantity found in river waters (Ward *et al.*, 2017). Hence,
46 floodplain vegetation, algae and floating macrophytes in highly productive and preserved
47 tropical areas, directly and rapidly provide organic and inorganic C to rivers (Abril *et al.*, 2014;
48 Sawakuchi *et al.*, 2017). Abril *et al.* (2014) further suggested that central Amazonian wetlands
49 export half of their gross primary production to rivers, being the primary sources for CO₂
50 outgassing by the Amazon.

51 Over the last decade, several studies successively updated regional and global estimates of river
52 C fluxes from land to oceans (Drake *et al.*, 2018). These studies underscored large data gaps
53 and uncertainties, suggesting that C fluxes might be much larger than previously thought. In
54 particular, uncertainties in the contribution of wetlands and macrophytes as a source of C for
55 rivers has been highlighted (Spencer *et al.*, 2013) and the need for new investigations identified.
56 Furthermore, river meandering, among other processes contributing to C input into rivers, river
57 meandering remains however a largely overlooked Earth surface process (Peixoto *et al.*, 2009).
58 Yet, this process is recognized in sculpting the Earth surface since more than 5 centuries, and
59 studies have recently pointed out its potential role in biogeochemical fluxes (Iepli & Lapôte,
60 2019). Abiotic factors, like sedimentary dynamics in meandering rivers, have been suggested
61 as essential than biotic factors, like productivity and respiration, in the terrestrial organic C
62 cycle (Torres *et al.*, 2017; Iepli & Lapôte, 2019).

63 Typically, meandering rivers are characterized by lateral bank erosion occurring at the outer
64 meander bends, whereas lateral accretion processes form point bars within inner meander bends
65 (Leopold and Wolman, 1960; Allen, 1965). Within the Amazon basin, lateral channel migration

66 generates meander scrolls forming a sequence of ridges and swales, on which a sequential
67 primary forest succession of high productivity rapidly takes place (Salo *et al.*, 1986; Junk *et al.*,
68 1989; Puhakka *et al.*, 1992). Forest succession, leading eventually to the mature stage, continues
69 when the channel further migrates and point bars are integrated into the floodplain. Conversely,
70 channel migration also causes bank erosion which in turn promotes direct massive inputs of
71 coarse woody material to river channels, thus providing substantial quantities of autochthonous
72 C, potentially exceeding those imported through litterfall and respiration. Active river
73 meandering closely linked to point bar formation, floodplain aging and lateral channel erosion,
74 thus presents a relevant Earth surface process to consider for accurately quantifying and
75 understanding floodplain C sequestration and its export to the aquatic continuum (Wohl *et al.*,
76 2013; Sutfin *et al.*, 2016).

77 Here, we aimed to provide evidence that river meandering in Amazonian floodplains
78 significantly contributes to river C budgets. Our objective was to quantify the amount of C that
79 annually accumulates in the forest biomass, as well as the part that is annually exported to the
80 river channel, within the active meander belt of the river, i.e. the area where contemporary
81 channel migration occurred. We investigated one of the major active tributaries of the Amazon,
82 the Ucayali River, Peru, over a period of 35 years (1984-2019). We used the yearly water
83 classification history dataset provided by the Joint Research Centre to produce annual maps of
84 point bar formation, floodplain ages and river channel erosion in the 1984-2019 active meander
85 belt. Annual maps were combined with a model predicting the living above-ground forest C
86 stock from the floodplain age to derive amounts of C annually fixed by net primary production
87 and exported to river waters after bank erosion. The quantity, quality and fate of the C provided
88 by Amazonian meandering rivers to the aquatic continuum is discussed in respect to the existing
89 literature.

90 **3. Method**

91 3.1. Study area

92 The Ucayali River is located in the western part of the Amazon basin (Fig. 1a). It is a major
93 tributary of the Amazon River extending approximately 900 km from its upstream confluence
94 with the Rio Tambo and Rio Urubamba to its downstream confluence with the Marañón River.
95 The mean annual water discharge is about $12\,100\text{ m}^3\text{ s}^{-1}$ and water depth between low and high
96 flood flows can range from 8 to 15 m (Santini *et al.*, 2019). The maximum and minimum
97 monthly flows, recorded over the 1996-2018 period at the Requena gauging station, is of 22 900
98 and $2\,500\text{ m}^3\text{ s}^{-1}$ respectively (HYBAM, 2020). Close to the town of Pucallpa, the floodplain
99 width is about 25 km and the active meander belt is approximately 10 km in width (Fig. 1b, c).
100 The Ucayali is considered as one of the last pristine free meandering white-water rivers
101 worldwide, characterized by high suspended sediment loads, nutrient-rich waters and high
102 lateral channel migration rates within an unconstrained, forested floodplain (Constantine *et al.*,
103 2014). Within meandering floodplain rivers, forest primary succession is distinctly age-zonated
104 (Salo *et al.*, 1986; Junk *et al.*, 1989; Puhakka *et al.*, 1992). The vegetation succession progresses
105 from early successional stages dominated by short-lived species to latter successional stages
106 dominated by long-lived species along a cross-river and age gradient (Salo *et al.*, 1986;
107 Lamotte, 1990; Fig. 2). The early stage of primary succession begins on newly formed alluvial
108 bars, mainly point bars, rapidly colonized by *Tessaria integrifolia* L. and *Gynerium sagittatum*,
109 forming dense canopies of about 5-8 m in height. This early pioneer stage is replaced by a
110 second stage dominated by *Cecropia tessmannii*, forming a closed canopy of about 14-18 m in
111 height. The *Cecropia* forest is located on older meander scrolls in backwater depressions.
112 During these two first stages, vegetation contributes to sediment and organic matter trapping,
113 which leads to floodplain construction and soil C sequestration (Fig. 2; Salo *et al.*, 1986). The
114 following stage is a mixed forest dominated by *Ficus insipida* and *Cedrela odorata*, forming a
115 closed canopy of about 20-25 m in height. At this stage, floodplain surface elevation is about 5

116 m above the low water level. Its topography is more homogeneous compared to the pioneer
117 zone in the previous stages of succession. This is due to the deposition of large amounts of silt
118 in backwater depressions during seasonal flooding. The later successional mixed forest is more
119 diversified and composed of large trees with a canopy of about 40 m in height. Soil topography
120 of the floodplain at this level (> 5-10 m above the low water level) is generally flat with only
121 minor remaining depressions. This forest succession trajectory is basically the same at each
122 meander of the Ucayali River (Kalliola *et al.*, 1991). Lateral channel erosion leads to a
123 continuous reset and regeneration of the primary vegetation succession over large areas (Salo
124 *et al.*, 1986; Kalliola *et al.*, 1991). Since point bars of the Ucayali River are either rapidly eroded
125 or integrated into the forested floodplain during lateral channel migration, we will, hereafter,
126 exclusively distinguish the river channel from its floodplain, including point bars.

127 3.2. Mapping floodplain formation, aging and erosion

128 We used the yearly water classification history dataset (v1.2) provided by the Joint Research
129 Centre (JRC) and freely available on the Google Earth Engine (GEE) platform (Gorelick *et al.*,
130 2017). This dataset was firstly created by Pekel *et al.* (2016) and now consists in 36 annual
131 raster maps spanning the 1984-2019 period. Pixels size approximately 900 m² at ground level
132 and are classified in ‘no data’, ‘non-water’, ‘seasonal water’ or ‘permanent water’ (Fig. S1 in
133 Appendix A). In order to create an envelope for data extraction, we firstly downloaded
134 geometries (i.e. polylines shapefiles) of the Ucayali River from the Open Street Map database
135 available at <https://download.geofabrik.de>. Then, we created a 10-km buffer across the river
136 using the ArcGIS software package (ESRI, Redland, USA). The yearly water classification
137 history dataset overlaying the river buffer was finally downloaded from the GEE platform.
138 Using the MatLab software package (Mathworks, Natick, USA), the 36 annual raster maps were
139 proceeded in order to map annual areas of floodplain formation, ages and erosion. The

140 algorithm was applied pixel-by-pixel and year-by-year as illustrated in Figure 3. Pixels that
141 were classified as ‘seasonal water’ or ‘permanent water’ at a given year (e.g. 1984; Fig. 3a),
142 and classified ‘non-water’ the following year (e.g. 1985), were mapped as 1-year-old pixels.
143 Each year from 1985 to 2019, every pixel age-determined at a given year (e.g. 1-year-old in
144 1985) and remaining ‘non-water’ the following year (e.g. 1986) was incremented with one
145 additional year (e.g. 2-year-old in 1986). Remaining ‘non-water’ and ‘no data’ pixels with no
146 age between successive years (e.g. between 1984 and 1985) were set to age ‘non-determined’
147 (ND). Typically, ND pixels corresponded to floodplain and upland areas created before 1984.
148 Each year, from 1985 to 2019, every pixel age-determined at a given year (e.g. 2-year-old in
149 1986) and classified ‘seasonal water’ or ‘permanent water’ the following year (e.g. 1987) was
150 considered as an eroded area (Fig. 3b) and reset to age 0 (e.g. 0-year-old in 1987).

151 3.3. Deriving C-stocks from floodplain ages

152 In line with Pahukka *et al.* (1992), we assumed that on the Ucayali River, pioneer vegetation
153 colonizes bare alluvial bars from the year of their creation (Fig. S2 in Appendix A). We thus
154 considered that the vegetation age is equal to the floodplain age. We used published data to
155 predict the forest above-ground carbon stock (C-stock in Mg C ha⁻¹) from the floodplain age
156 (age in years), and constructed a model predicting C-stock as a function of age (Fig. 3c). The
157 data were published by Schöngart and Wittmann (2010) and based upon thousands of in situ
158 vegetation structure inventories and tree ring measurements within floodplains of central
159 Amazonia. Forest above-ground carbon stocks were estimated in several, almost undisturbed
160 successional stages, with stands varying between 7 and 240 years of age. Forest structure data
161 and several allometric models were used to construct a data series of C-stocks per forest age.
162 First, we extracted data from the figure 18.10 presented by Schöngart and Wittmann (2010)
163 using Web Plot Digitizer 4.3 software (Ankit Rohatgi, Pacifica, California, USA). Second, we

164 fitted a 3rd order polynomial model to the 35 first years of the data series. These 35 years
165 corresponded to the forest establishment that we analysed on the Ucayali River between 1984
166 and 2019. For floodplain forests established before 1984 (ND ages; Fig. 3a, b), we assumed a
167 constant C-stock, i.e. old-growth forests with ages > 70-year-old in the data series. This
168 assumption was based on the floodplain age structure of eroded outer meander bends presented
169 in the results section.

170 3.4. Annual accumulation of floodplain forest C-stocks and its erosion

171 Floodplain areas were converted into above-ground forest C-stocks based on our model (Fig.
172 3c). The annual total C-stock (in Mg C ha⁻¹) was obtained by summing C-stocks of all vegetated
173 floodplain ages since 1984. An annual C accumulation rate was obtained by (1) subtracting the
174 total C-stock of year n by the one of year n-1, and (2) by applying a linear regression and the
175 calculation of the root mean square error (RMSE). C-accumulation in floodplain and upland
176 forest areas established before 1984 were not considered in the present study because they were
177 outside of the 1984-2019 active-meander belt. Annual C-stock lost through floodplain erosion
178 was obtained by summing eroded C-stocks of determined and non-determined (ND) floodplain
179 ages.

180 4. Results

181 4.1. Annual vegetated floodplain area formation and erosion

182 Over the 1984-2019 period, the water surface area of the Ucayali River accounted for 220 ± 25
183 $\times 10^3$ ha (annual average and its standard deviation; Appendix B). Maximum water surface area
184 extensions were observed in 1988, 1994, 2001, 2011, 2017 and minimums in 1987, 1992, 1997,
185 2005, 2010, 2013 and 2018 (Fig. 4a). Negative anomalies appeared mainly before 2000 and
186 positives anomalies mainly after 2000. Yearly formation of floodplain areas occurred mainly

187 within inner meander bends and accounted in average for $19.0 \pm 7.7 \times 10^3 \text{ ha}^{-1} \text{ yr}^{-1}$ (Fig. 4b; Fig.
188 5; Appendix B and C). Conversely, floodplain erosion was located mainly in outer meander
189 bends and closely balanced floodplain formation with an average of $19.8 \pm 6.7 \times 10^3 \text{ ha}^{-1} \text{ yr}^{-1}$
190 (Fig. 4c; Appendix B and C).

191 4.2. Age structure of vegetated floodplain areas

192 We found that meandering promotes rejuvenation and recurrent formation of large areas of bare
193 alluvial bars that are quickly colonized by pioneer vegetation. Over the 1984-2019 period, ages
194 of floodplain areas were unevenly distributed (Fig. 6a). One-year-old floodplain areas largely
195 dominated. However, about 1/3 of these newly formed floodplain areas were eroded the
196 following year. Indeed, we found that older age classes generally decreased in areas following
197 a negative logarithmic trend (Fig. 6a). This trend resulted from floodplain erosion (Fig. 6b).
198 Newly established floodplain areas at inner meander bends were primarily affected by erosion
199 at a rate of $6.4 \pm 3.3 \times 10^3 \text{ ha}^{-1} \text{ yr}^{-1}$, i.e. 1/3 of the yearly formed floodplain surface area
200 ($19.0 \pm 7.7 \times 10^3 \text{ ha}^{-1} \text{ yr}^{-1}$). The rate of erosion decreased from younger to older floodplain areas
201 (Fig. 6b). Floodplain erosion occurred equally in outer meander bends and in areas established
202 before 1984, i.e. non-determined in age (ND) in the present study. Erosion in areas of ND ages
203 accounted annually for about $7.0 \pm 3.8 \times 10^3 \text{ ha}^{-1} \text{ yr}^{-1}$ (Fig. 6b; ND).

204 4.3. Annual changes in floodplain forest C-stocks

205 Our model used to derive C-stocks from floodplain ages showed a very good adjustment to the
206 data ($R^2 = 0.99$; Fig. 7). One-year-old vegetation accounted for an average of 0.7 Mg C ha^{-1} and
207 increased to $95.3 \text{ Mg C ha}^{-1}$ at 35-year-old. Old-growth floodplain forests, i.e. those that
208 established on areas older than 70-year-old, levelled off at nearly 115 Mg C ha^{-1} (Fig. 7). We
209 combined annual maps of floodplain ages with our C-stock model and produced annual maps
210 of above-ground C-stocks (Fig. 8). The mean annual C accumulation rate of floodplain forests

211 established after 1984 in the Ucayali 1984-2019 active meander belt was estimated at 0.01×10^6
212 Mg C yr^{-1} with a RMSE of $0.04 \times 10^6 \text{ Mg C yr}^{-1}$ (Fig. 9a). Given the relation between available
213 floodplain area and C-stock, the generation with the most effective C-sequestration capacity
214 was the 23-year-old forest (Fig. 9b). Annual floodplain erosion caused by lateral channel
215 migration accounted approximately for $0.9 \pm 0.4 \times 10^6 \text{ Mg C yr}^{-1}$ (Fig. 10a). Floodplain areas
216 which established before 1984 largely dominated eroded C-stocks with $0.8 \pm 0.4 \times 10^6 \text{ Mg C yr}^{-1}$
217 1 (ND; Fig. 10b).

218 **5. Discussion**

219 5.1. Annual floodplain formation balances annual floodplain erosion in area but not in C 220 budget

221 We found that rates of annual floodplain formation and rates of annual floodplain erosion
222 appeared to be in balance over time with $19.0 \pm 7.7 \times 10^3 \text{ ha}^{-1} \text{ yr}^{-1}$ and $19.8 \pm 6.7 \times 10^3 \text{ ha}^{-1} \text{ yr}^{-1}$,
223 respectively. Our results confirm those reported by Puhakka *et al.* (1992) who showed that outer
224 banks and point bars have, respectively, roughly equivalent rates of erosion and sediment
225 deposition, maintaining a relatively constant channel width. Similarly, Peixoto *et al.* (2009) and
226 Schwenk *et al.* (2017) reported an annual balance of erosion and deposition over large study
227 areas and multidecadal periods. Peixoto *et al.* (2009) suggested that annual release of C caused
228 by river dynamics would be much higher than the C annually sequestered within the floodplain.
229 Our results have quantitatively confirmed their hypothesis. Indeed, within the 1984-2019 active
230 meander belt of the Ucayali River, the floodplain forest annually accumulates $0.01 \pm 0.04 \times 10^6$
231 Mg C yr^{-1} and exports $0.9 \pm 0.4 \times 10^6 \text{ Mg C yr}^{-1}$. Although it appeared that there is a balance in
232 areas between floodplain formation and erosion, we show that there is however a strong
233 imbalance in rates of floodplain forest C fixation and export to river waters caused by lateral

234 channel migration. This imbalance is mainly due to massive erosion of old-growth floodplain
235 forests with high C-stock densities (about 115 Mg C ha⁻¹).

236 5.2. Lateral channel migration as a significant C provider to the aquatic continuum

237 There are multiple C sources for the aquatic continuum, i.e. between aquatic ecosystems from
238 the atmosphere, headwater streams and inland waters, to coastal and marine systems. First, the
239 C conveyed to streams and rivers can be provided during precipitation where water drops can
240 be enriched in dissolved and particulate organic C (DOC, POC; Ward *et al.*, 2017). Then, when
241 entering forest canopies, drops capture DOC and POC at the surface of leaves, branches and
242 trunks. By instance, in the Rio Negro region, throughfall fluxes of 27.5 kg C ha⁻¹ yr⁻¹ have been
243 reported (Filoso *et al.*, 1999). Throughfall fluxes that range between 68.4 and 195.1 kg C ha⁻¹
244 yr⁻¹ and stem flow fluxes of 1.5 kg ha⁻¹ yr⁻¹ have been also reported in Amazonia (Neu *et al.*,
245 2016). In addition to the C provided by rainfall, root and canopy litterfall and respiration in
246 floodplain forests together with algal and floating macrophyte communities are considered as
247 the main C pathways to the aquatic continuum (Ward *et al.*, 2017).

248 Even though they represent only about 14 % of the Amazon basin, floodplains are highly
249 productive compared to terrestrial uplands and are hydrologically connected to river channels
250 during yearly overbank flooding (Richey *et al.*, 1980; Junk, 1985; Hoffmann *et al.*, 2009). It
251 has been reported that in Central Amazonia, floodplains can provide an amount of 59.6±38.7
252 Mg C ha⁻¹ yr⁻¹ to the channel network and streamflow (Abril *et al.*, 2014). Here, we point out
253 that lateral channel erosion is a crucial and overlooked physical driver delivering large amounts
254 of C to rivers. We show that channel migration in the upper Amazonian floodplain provides
255 between 0.7 and 115 Mg C ha⁻¹ yr⁻¹ to streamflow depending on the age of the forested
256 floodplain areas eroded. Over the studied period and area, we found that in average 44.7±21.4
257 Mg C ha⁻¹ yr⁻¹ was delivered by lateral channel erosion to the aquatic continuum (0.9±0.4×10⁶

258 Mg C yr⁻¹ delivered over $19.8 \pm 6.7 \times 10^3$ ha⁻¹ yr⁻¹). Our result is roughly equivalent to the amount
259 provided by the entire wetland system of the central Amazonian floodplain (i.e. flooded forest
260 and macrophytes litterfall and respiration; 59.6 ± 38.7 Mg C ha⁻¹ yr⁻¹), and roughly 10 times
261 higher than the amount of the woody part considered by Abril *et al.* (2014) i.e. 5.3 ± 2 Mg C
262 ha⁻¹ yr⁻¹.

263 The amount of C provided by meandering rivers is dependant on annual rates of floodplain
264 erosion. In the Amazon basin, different rates of channel migration of white-water rivers have
265 been observed to exponentially increase from east to west (Kalliola *et al.*, 1992; Mertes *et al.*,
266 1995; Peixoto *et al.*, 2009; Salo and Räsänen, 1989). Therefore, inputs of woody materials as a
267 consequence of lateral channel erosion may certainly increase along a downstream-upstream
268 gradient. Further studies are thus required to quantify the spatial variability and overall
269 contribution of Amazonian meandering rivers. Here, we have calculated the contribution of
270 above-ground forest biomass to streamflow, but further amounts of C input may originate from
271 (i) eroded floodplain soils (i.e. belowground total organic matter; Fig. 2), and (ii) the Andean
272 mountains situated upstream the study area, where torrential streams potentially accumulate
273 and transport large amounts of coarse woody debris provided by landslides occurring in
274 particular during tropical storm events (McClain and Naiman, 2008; Clark *et al.*, 2013; Wohl
275 and Ogden, 2013).

276 5.3. Nature and fate of the C provided by meandering rivers

277 The nature of the C that is annually exported into the aquatic continuum is a fundamental aspect
278 when considering the fate of this C and its role in the global cycle. It is usually considered that
279 river C is advected downstream and returned to the atmosphere *via* degassing by both microbial
280 and photochemical activity, ultimately resulting in a net zero exchange, especially in the tropics
281 where warm temperatures stimulate organic matter decomposition (Raymond *et al.*, 2013; Ward

282 *et al.*, 2013). For instance, Abril *et al.* (2014) proposed that central Amazonian waters receive
283 at least as much C from wetlands as they emit to the atmosphere, making a nearly neutral
284 balance in atmosphere-biosphere CO₂ exchanges. However, the C provided by meandering
285 rivers of the upper Amazon basin most probably differs from the C provided by wetlands of the
286 central Amazon. On the one hand, it has been shown for wetlands of the central Amazon that
287 the microbial communities decompose young organic C (> 5-year-old; Mayorga *et al.*, 2005;
288 Abril *et al.*, 2014). On the other hand, the organic C found in the water column mainly originates
289 from litterfall with low lignin content (Mayorga *et al.*, 2005; Abril *et al.*, 2014). Our results
290 suggest that in free meandering Amazonian rivers, such as the Ucayali River, older lignin is
291 present in substantial quantities. Higher concentrations of lignin are found in tree trunks,
292 branches and roots of ligneous terrestrial plants, and we estimated that mature and old growth
293 floodplain forests accounted for nearly half of the eroded floodplain area within the Ucayali
294 1984-2019 meander belt (Fig. 6b). However, the fate of these large C quantities of lignin
295 remains still uncertain. One hypothesis could be that this C is mineralized by microbial and
296 photochemical activity and/or exported downstream the aquatic continuum and/or accumulated
297 in the river sediment. Following Ward *et al.* (2013), half of these quantities could be degraded
298 and mineralized in the Amazon River. Anyhow, according to Galy *et al.* (2015), the erosion
299 and transportation capacities of rivers are to be considered as the main control of the biospheric
300 C export to oceans. Many large water storage reservoirs have been recently proposed for the
301 Amazon Basin (Finer and Jenkins, 2012). Since meandering rivers are known to be highly
302 sensitive to the disruption of sediment supply caused by such engineering projects (Constantine
303 *et al.*, 2014), it is highly suspected that such human infrastructures will greatly alter the natural
304 C fluxes we have here quantified.

305 **6. Conclusion**

306 Although the area of the Ucayali's 1984-2019 meander belt represents only a small fraction of
307 the Amazonian basin area, it significantly contributes to the amount of C that is transferred from
308 the floodplain forest to the aquatic continuum. The amount of woody C per unit area provided
309 by floodplain erosion caused by lateral channel erosion is nearly ten-fold higher than that
310 provided by central Amazon wetlands. Extrapolation of our results suggests that free
311 meandering white-water rivers may act as major agent in the global C cycle. These findings
312 point to the importance to quantify the overall contribution of free meandering forested
313 floodplain rivers worldwide to the global C cycle. In addition to variations in channel migration
314 rates, different floodplain tree species may show contrasting C-stock potentials and related
315 forest carbon export rates according to climate zones and biogeographical regions.

316 **7. Author contributions**

317 **Romain Wacker:** Conceptualization, Methodology, Formal analysis, Writing- Original draft
318 preparation. **Dov Corenblit:** Original Idea, Supervision, Conceptualization, Writing- Original
319 draft preparation. **Frédéric Julien:** Writing - Review & Editing. **Jean-Michel Martinez:**
320 Writing - Review & Editing. **Johannes Steiger:** Writing - Review & Editing.

321 **8. Competing interest statement**

322 The authors have no competing interests to declare.

323 **9. Acknowledgements**

324 RW acknowledges financial support from the French National Research Agency through an
325 Investissement d'Avenir (Labex CEBA, ref. ANR-10-LABX-25-01).

326 **10. References**

- 327 Abril, G., Martinez, J.-M., Artigas, L. F., Moreira-Turcq, P., Benedetti, M. F., Vidal, L.,
328 Meziane, T., Kim, J.-H., Bernardes, M. C., Savoye, N., Deborde, J., Souza, E. L.,
329 Albéric, P., Landim de Souza, M. F., & Roland, F. (2014). Amazon River carbon
330 dioxide outgassing fuelled by wetlands. *Nature* **505**, 395–398.
331 <https://doi.org/10.1038/nature12797>
- 332 Allen, J.R.L. (1965) A review of the origin and characteristics of recent alluvial sediments.
333 *Sedimentology* **5**, 89-191.
- 334 Clark, K. E., Hilton, R. G., West, A. J., Malhi, Y., Gröcke, D. R., Bryant, C. L., Ascough, P.
335 L., Robles Caceres, A., & New, M. (2013). New views on “old” carbon in the Amazon
336 River: Insight from the source of organic carbon eroded from the Peruvian Andes.
337 *Geochemistry, Geophysics, Geosystems* **14**, 1644–1659.
338 <https://doi.org/10.1002/ggge.20122>
- 339 Constantine, J. A., Dunne, T., Ahmed, J., Legleiter, C., & Lazarus, E. D. (2014). Sediment
340 supply as a driver of river meandering and floodplain evolution in the Amazon Basin.
341 *Nature Geoscience* **7**, 899–903. <https://doi.org/10.1038/ngeo2282>
- 342 Drake, T. W., Raymond, P. A., Spencer, R. G. M. (2018) Terrestrial carbon inputs to inland
343 waters: A current synthesis of estimates and uncertainty. *Limnology and Oceanography*
344 *Letters* **3**, 123–142. <https://doi.org/10.1002/lol2.10055>
- 345 Feng, X., Feakins, S. J., Liu, Z., Ponton, C., Wang, R. Z., Karkabi, E., Galy, V., Berelson, W.
346 M., Nottingham, A. T., Meir, P., & West, A. J. (2016). Source to sink: Evolution of
347 lignin composition in the Madre de Dios River system with connection to the Amazon
348 basin and offshore. *Journal of Geophysical Research : Biogeosciences* **121**, 1316–1338.
349 <https://doi.org/10.1002/2016JG003323>
- 350 Filoso, S., Williams, M. R., & Melack, J. M. (1999). Composition and deposition of throughfall
351 in a flooded forest archipelago. *Biogeochemistry* **45**, 169–195.
352 <https://doi.org/10.1023/A:1006108618196>
- 353 Finer M, Jenkins CN (2012) Proliferation of Hydroelectric Dams in the Andean Amazon and
354 Implications for Andes-Amazon Connectivity. *PLoS ONE* **7**(4): e35126.
355 <https://doi.org/10.1371/journal.pone.0035126>
- 356 Galy, V., Peucker-Ehrenbrink, B., & Eglinton, T. (2015). Global carbon export from the
357 terrestrial biosphere controlled by erosion. *Nature* **521**, 204–207.
358 <https://doi.org/10.1038/nature14400>
- 359 Gorelick, N., Hancher, M., Dixon, M., Ilyushchenko, S., Thau, D., & Moore, R. (2017). Google
360 Earth Engine: Planetary-scale geospatial analysis for everyone. *Remote Sensing of*
361 *Environment* **202**, 18–27. <https://doi.org/10.1016/j.rse.2017.06.031>
- 362 Hoffmann, T., Glatzel, S., & Dikau, R. (2009). A carbon storage perspective on alluvial
363 sediment storage in the Rhine catchment. *Geomorphology*, **108**, 127–137.
364 <https://doi.org/10.1016/j.geomorph.2007.11.015>
- 365 HYBAM, www.sno-hybam.org, last access at 01/12/2020.
- 366 Junk, W. J. (1985). The Amazon floodplain—a sink or source for organic carbon. *Mitteilungen*
367 *aus dem Geologische-Palaontologische Institut der Universität Hamburg*.
368 *SCOPE/UNEP Sonderband* **58**, 267–283.
- 369 Junk, Wolfgang J., Bayley, Peter B., Sparks, R. (1989). The flood pulse concept in river-
370 floodplain systems. In *Canadian Journal of Fisheries and Aquatic Science*, **106**, 10–
371 127.
- 372 Kalliola, R., Salo, J., Puhakka, M., & Rajasilta, M. (1991). New Site Formation and Colonizing
373 Vegetation in Primary Succession on the Western Amazon Floodplains. *The Journal of*
374 *Ecology* **79**, 877–901. <https://doi.org/10.2307/2261087>
- 375 Kalliola, R., Salo, J., Puhakka, M., Rajasilta, M., Häme, T., Neller, R.J., E. Räsänen M.E., &
376 Danjoy Aria, W.A. (1992) Upper Amazon channel migration: implications for

377 vegetation disturbance and succession using bitemporal Landsat MSS images.
378 *Naturwissenschaften* **79**, 75–79.

379 Lamotte, S. (1990). Fluvial dynamics and succession in the Lower Ucayali River basin,
380 Peruvian Amazonia. *Forest Ecology and Management* **33**, 141–156.

381 Ielpi, A., Lapôtre, M. G. A. (2019) A tenfold slowdown in river meander migration driven by
382 plant life. *Nature Geoscience* **13**, 82–86. <https://doi.org/10.1038/s41561-019-0491-7>

383 Leopold, L.B. & Wolman, M.G. (1960) River meanders. *Geological Society of America*
384 *Bulletin* **71**, 769-794.

385 Mayorga, E., Aufdenkampe, A. K., Masiello, C. A., Krusche, A. V., Hedges, J. I., Quay, P. D.,
386 Richey, J. E., & Brown, T. A. (2005). Young organic matter as a source of carbon
387 dioxide outgassing from Amazonian rivers. *Nature* **436**, 538–541.
388 <https://doi.org/10.1038/nature03880>

389 McClain, M. E., & Naiman, R. J. (2008). Andean influences on the biogeochemistry and
390 ecology of the Amazon River. *BioScience* **58**, 325–338.
391 <https://doi.org/10.1641/B580408>

392 Mertes, L. A. K., Daniel, D. L., Melack, J. M., Nelson, B., Martinelli, L. A., & Forsberg, B. R.
393 (1995). Spatial patterns of hydrology, geomorphology, and vegetation on the floodplain
394 of the Amazon river in Brazil from a remote sensing perspective. *Geomorphology* **13**,
395 215-232 [https://doi.org/10.1016/0169-555X\(95\)00038-7](https://doi.org/10.1016/0169-555X(95)00038-7)

396 Neu, V., Ward, N. D., Krusche, A. V., & Neill, C. (2016). Dissolved organic and inorganic
397 carbon flow paths in an amazonian transitional forest. *Frontiers in Marine Science* **3**
398 <https://doi.org/10.3389/fmars.2016.00114>

399 Peixoto, J. M. A., Nelson, B. W., Wittmann, F. (2009) Spatial and temporal dynamics of river
400 channel migration and vegetation in central Amazonian white-water floodplains by
401 remote-sensing techniques. *Remote Sensing of Environment* **113**, 2258–2266.
402 <http://dx.doi.org/10.1016/j.rse.2009.06.015>

403 Pekel, J. F., Cottam, A., Gorelick, N., & Belward, A. S. (2016). High-resolution mapping of
404 global surface water and its long-term changes. *Nature* **540**, 418–422.
405 <https://doi.org/10.1038/nature20584>

406 Puhakka, M., Kalliola, R., Rajasilta, M., & Salo, J. (1992). River Types, Site Evolution and
407 Successional Vegetation Patterns in Peruvian Amazonia. *Journal of Biogeography*.
408 <https://doi.org/10.2307/2845707>

409 Raymond, P. A., Hartmann, J., Lauerwald, R., Sobek, S., McDonald, C., Hoover, M., Butman,
410 D., Striegl, R., Mayorga, E., Humborg, C., Kortelainen, P., Dürr, H., Meybeck, M.,
411 Ciais, P., & Guth, P. (2013). Global carbon dioxide emissions from inland waters.
412 *Nature* **503**, 355–359. <https://doi.org/10.1038/nature12760>

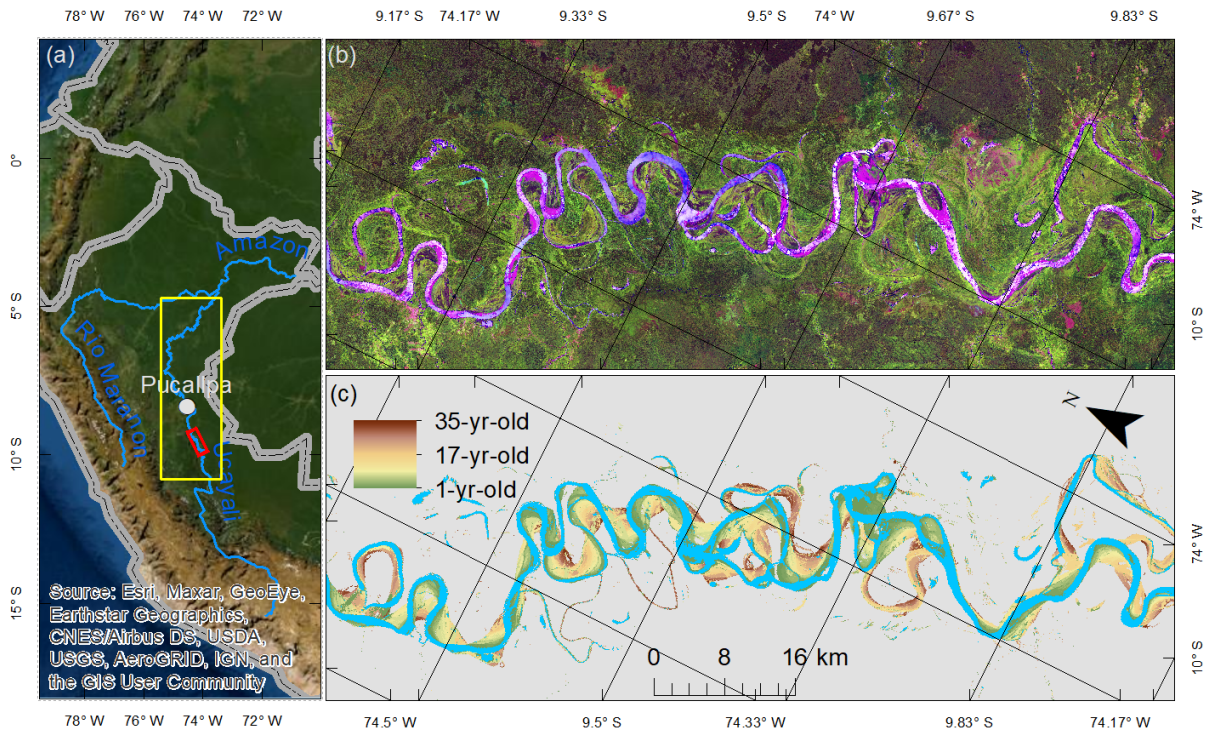
413 Richey, J. E., Brock, J. T., Naiman, R. J., Wissmar, R. C., & Stallard, R. F. (1980). Organic
414 carbon: oxidation and transport in the Amazon River. *Science* **207**, 1348-1351.
415 <https://doi.org/10.1126/science.207.4437.1348>

416 Salo, J., Kalliola, R., Häkkinen, I., Mäkinen, Y., Niemelä, P., Puhakka, M., & Coley, P. D.
417 (1986). River dynamics and the diversity of Amazon lowland forest. *Nature* **322**, 254–
418 258. <https://doi.org/10.1038/322254a0>

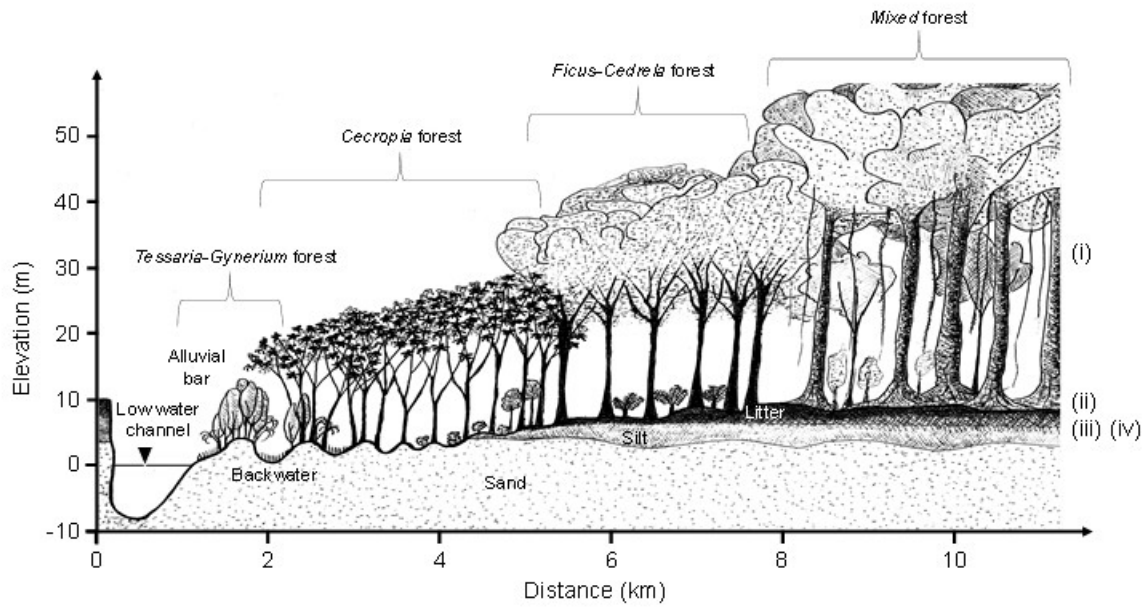
419 Salo, J., & Räsänen, M. (1989). Hierarchy of landscape patterns in western Amazon. In: Holm-
420 Nielsen, L.B., Nielsen, I.C., Balslev, H. (eds) Tropical forests: Botanical dynamics,
421 speciation and diversity, Academic Press, London.

422 Santini, W., Camenen, B., Le Coz, J., Vauchel, P., Guyot, J. L., Lavado, W., Villar, R. E., Julien
423 F. & Martinez J.M. (2019). An index concentration method for suspended load
424 monitoring in large rivers of the Amazonian foreland. *Earth Surface Dynamics* **7**, 515-
425 536. <https://doi.org/10.5194/esurf-7-515-2019>

- 426 Sawakuchi, H. O., Neu, V., Ward, N. D., Barros, M. de L. C., Valerio, A. M., Gagne-Maynard,
427 W., Cunha, A. C., Less, D. F. S., Diniz, J. E. M., Brito, D. C., Krusche, A. V., & Richey,
428 J. E. (2017). Carbon dioxide emissions along the lower Amazon River. *Frontiers in*
429 *Marine Science* **4**. <https://doi.org/10.3389/fmars.2017.00076>
- 430 Schöngart J., Wittmann F. (2010) Biomass and Net Primary Production of Central Amazonian
431 Floodplain Forests. In: Junk W., Piedade M., Wittmann F., Schöngart J., Parolin P. (eds)
432 Amazonian Floodplain Forests. Ecological Studies (Analysis and Synthesis), vol 210.
433 Springer, Dordrecht. https://doi.org/10.1007/978-90-481-8725-6_18
- 434 Schwenk, J., Khandelwal, A., Fratkin, M., Kumar, V., & Foufoula-Georgiou, E. (2017). High
435 spatiotemporal resolution of river planform dynamics from landsat: The rivMAP
436 toolbox and results from the Ucayali river. *Earth and Space Science* **4**, 46–75.
437 <https://doi.org/10.1002/2016EA000196>
- 438 Spencer, R. G. M., Aiken, G. R., Dornblaser, M. M., Butler, K. D., Holmes, R. M., Fiske, G.,
439 Mann, P. J., Stubbins, A. (2013) Chromophoric dissolved organic matter export from
440 US rivers. *Geophysical Research Letters* **40**, 1575–1579.
441 <https://doi.org/10.1002/grl.50357>
- 442 Sutfin, N. A., Wohl, E. E., & Dwire, K. A. (2016). Banking carbon: A review of organic carbon
443 storage and physical factors influencing retention in floodplains and riparian
444 ecosystems. *Earth Surface Processes and Landforms* **41**, 38–60.
445 <https://doi.org/10.1002/esp.3857>
- 446 Torres, M. A., Limaye, A. B., Ganti, V., Lamb, M. P., West, A. J., Fischer, W. W. (2017) Model
447 predictions of long-lived storage of organic carbon in river deposits. *Earth Surface*
448 *Dynamics* **5**, 711–730. <https://doi.org/10.5194/esurf-5-711-2017>
- 449 Ward, N. D., Bianchi, T. S., Medeiros, P. M., Seidel, M., Richey, J. E., Keil, R. G., &
450 Sawakuchi, H. O. (2017). Where Carbon Goes When Water Flows: Carbon Cycling
451 across the Aquatic Continuum. *Frontiers in Marine Science* **4**.
452 <https://doi.org/10.3389/fmars.2017.00007>
- 453 Ward, N. D., Keil, R. G., Medeiros, P. M., Brito, D. C., Cunha, A. C., Dittmar, T., Yager, P.
454 L., Krusche, A. V., & Richey, J. E. (2013). Degradation of terrestrially derived
455 macromolecules in the Amazon River. *Nature Geoscience* **6**, 530–533.
456 <https://doi.org/10.1038/ngeo1817>
- 457 Wohl, E., & Ogden, F. L. (2013). Organic carbon export in the form of wood during an extreme
458 tropical storm, Upper Rio Chagres, Panama. *Earth Surface Processes and Landforms*,
459 **38**, 1407–1416. <https://doi.org/10.1002/esp.3389>
- 460 Wohl, E., Dwire, K., Sutfin, N., Polvi, L., & Bazan, R. (2012). Mechanisms of carbon storage
461 in mountainous headwater rivers. *Nature communications* **3**, 1–8.
462



464
 465 **Figure 1** The freely meandering Ucayali River in the upper Amazonian region, Peru. **(a)**
 466 Location map: the yellow rectangle indicates the extent of the study area and the red rectangle
 467 indicates the extensions of panels (b) and (c), located approximately 120 km upstream of
 468 Pucallpa, Peru. **(b)** False colour composite satellite image showing the Ucayali meander belt
 469 extension in light green. This cloud-free satellite Landsat 8 image was obtained through the
 470 selection of the greenest pixels over the year 2018. The first short wave infra-red satellite band
 471 was affected to the red colour on screen, the near infra-red band to the green and the red band
 472 to the blue. **(c)** Floodplain ages range from 1-year (green colour) to 35-year (brown colour)
 473 within the 1984-2019 meander belt. Blue and grey colours correspond respectively to surface
 474 water and upland areas formed before 1984 (non-determined ages), respectively.
 475

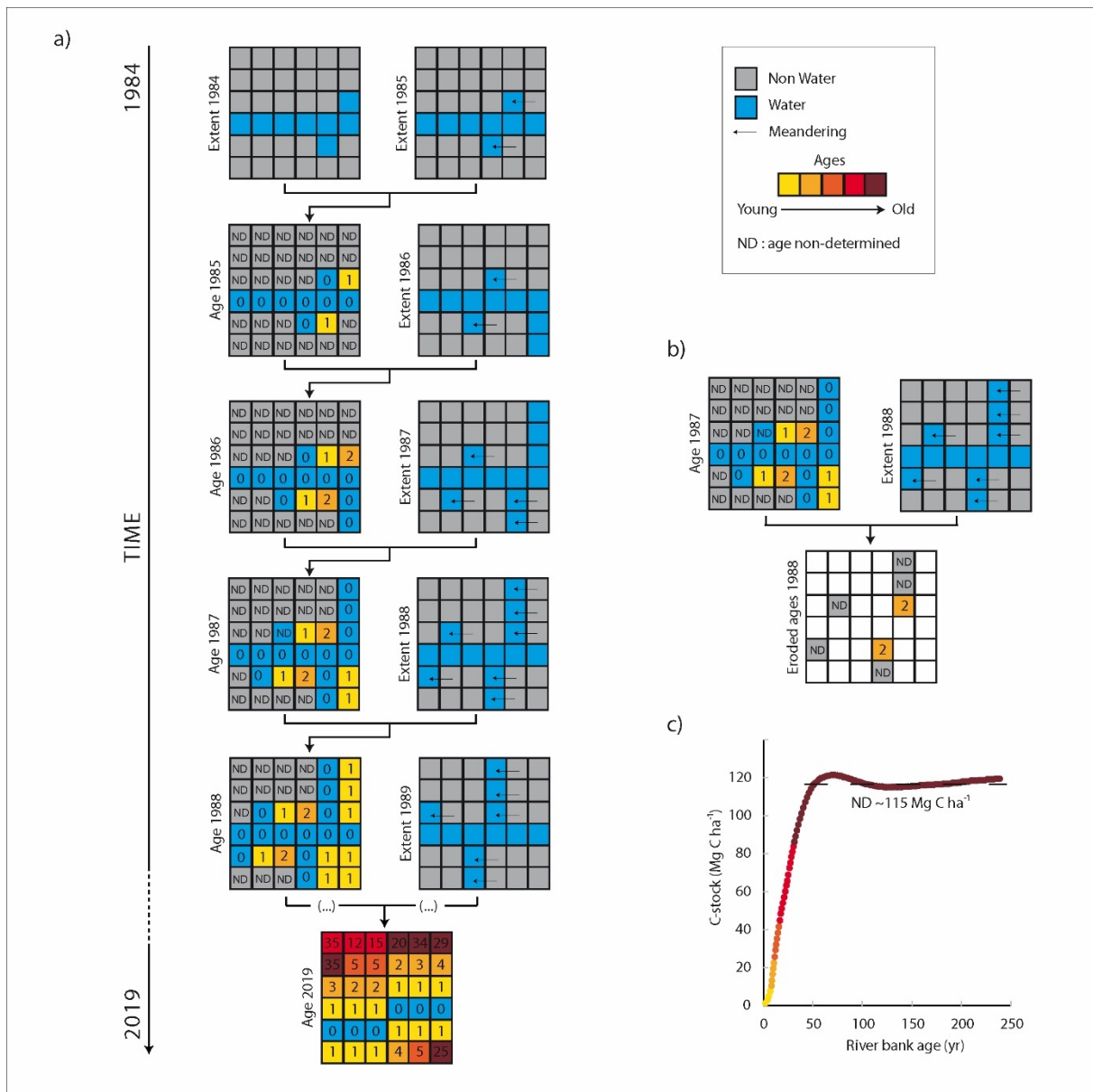


477

478 **Figure 2** Simplified model of the floodplain vegetation succession in the study area which
 479 comprises four main interrelated carbon reservoirs (modified from Salo *et al.*, 1986; Kayranli
 480 *et al.*, 2010; Stufin *et al.*, 2016): (i) aboveground living terrestrial and seasonally flooded forest
 481 biomass (trunk, branches and foliage); (ii) aboveground necromass (dead wood and litter); (iii)
 482 belowground living biomass (roots and micro-organisms); and (iv) total organic matter in the
 483 soil (decomposed dead organic flora and fauna). The present study focused on the first carbon
 484 reservoir of the floodplain, i.e. aboveground living terrestrial and seasonally flooded forest
 485 biomass.

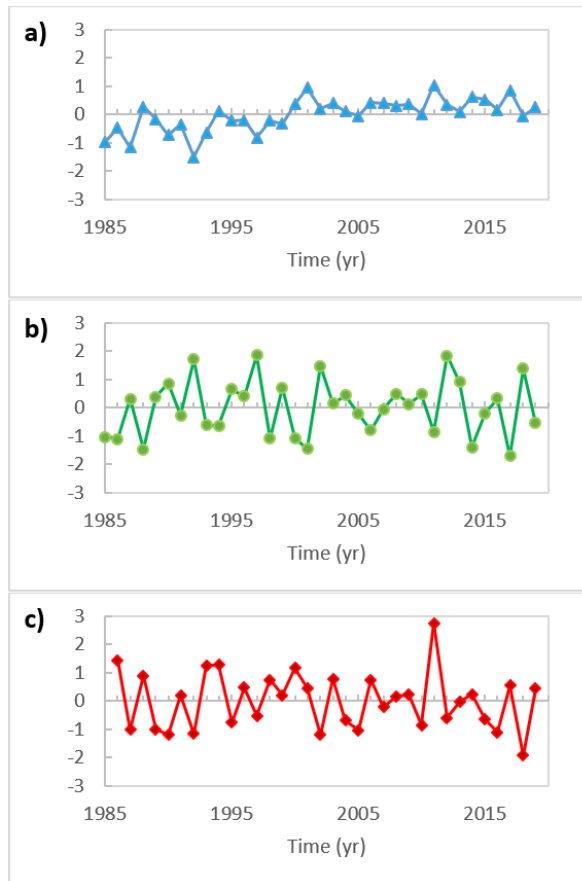
486

487



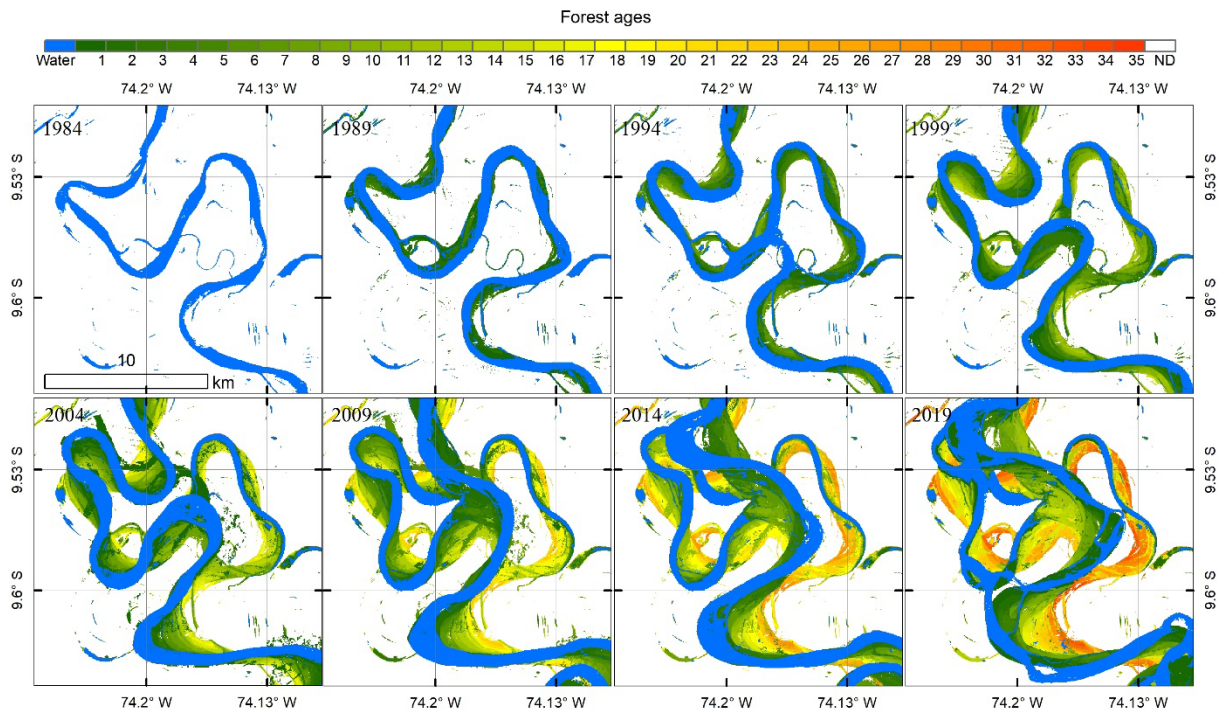
488

489 **Figure 3** Conceptual approach used to derive forest above ground carbon stock (C-stock) from
 490 floodplain area age. **a)** Pixel-by-pixel and year-by-year algorithm used to obtain yearly maps
 491 of area ages based on the analysis of the yearly water classification history dataset (Pekel *et al.*,
 492 2016). **b)** Pixel-by-pixel and year-by-year algorithm used to obtain yearly maps of eroded
 493 floodplain area ages. **c)** Data series used to model and derive C-stocks from floodplain area
 494 ages (Schöngart and Wittmann, 2010).
 495



496

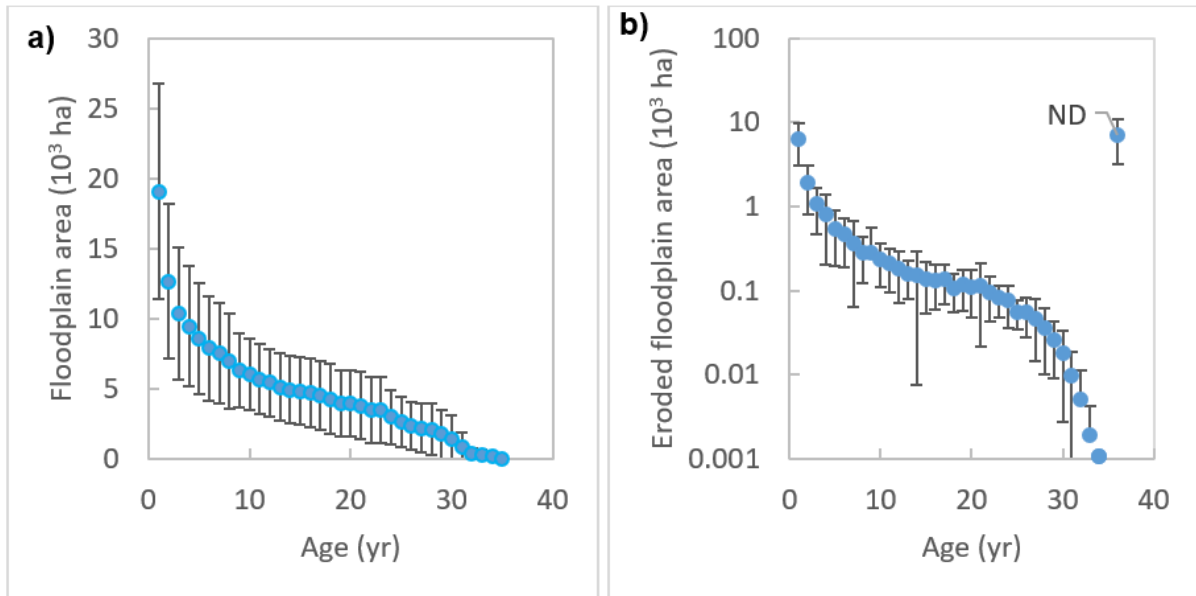
497 **Figure 4** Annual area fluctuations of **a)** water surfaces, **b)** floodplain formation and **c)**
 498 floodplain erosion between 1984 and 2019. Values are standardized, i.e. the 1984-2019 average
 499 was subtracted and the result was divided by the 1984-2019 standard deviation.
 500



501

502 **Figure 5** River meandering and floodplain forest dynamics according to a 5-yr time interval
 503 between 1984 and 2019 in the vicinity of Sampaya (Peru). Annual maps were created using the
 504 algorithm described in Fig. 3a. Non-eroded, remaining floodplain and upland forests which
 505 established before 1984 are indicated as age non-determined (ND; white colour).
 506

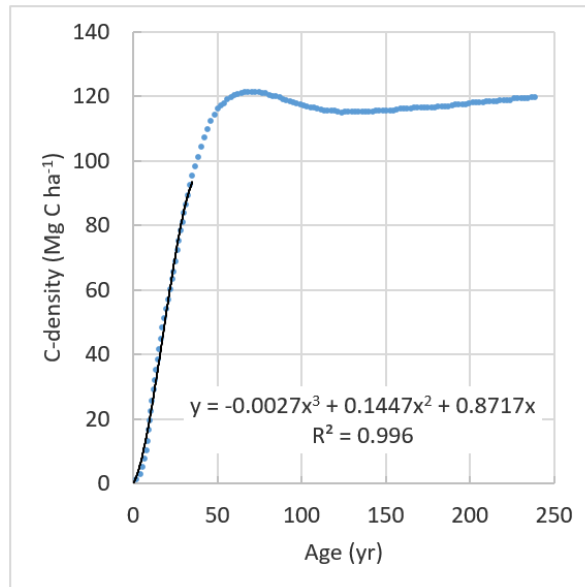
507



508

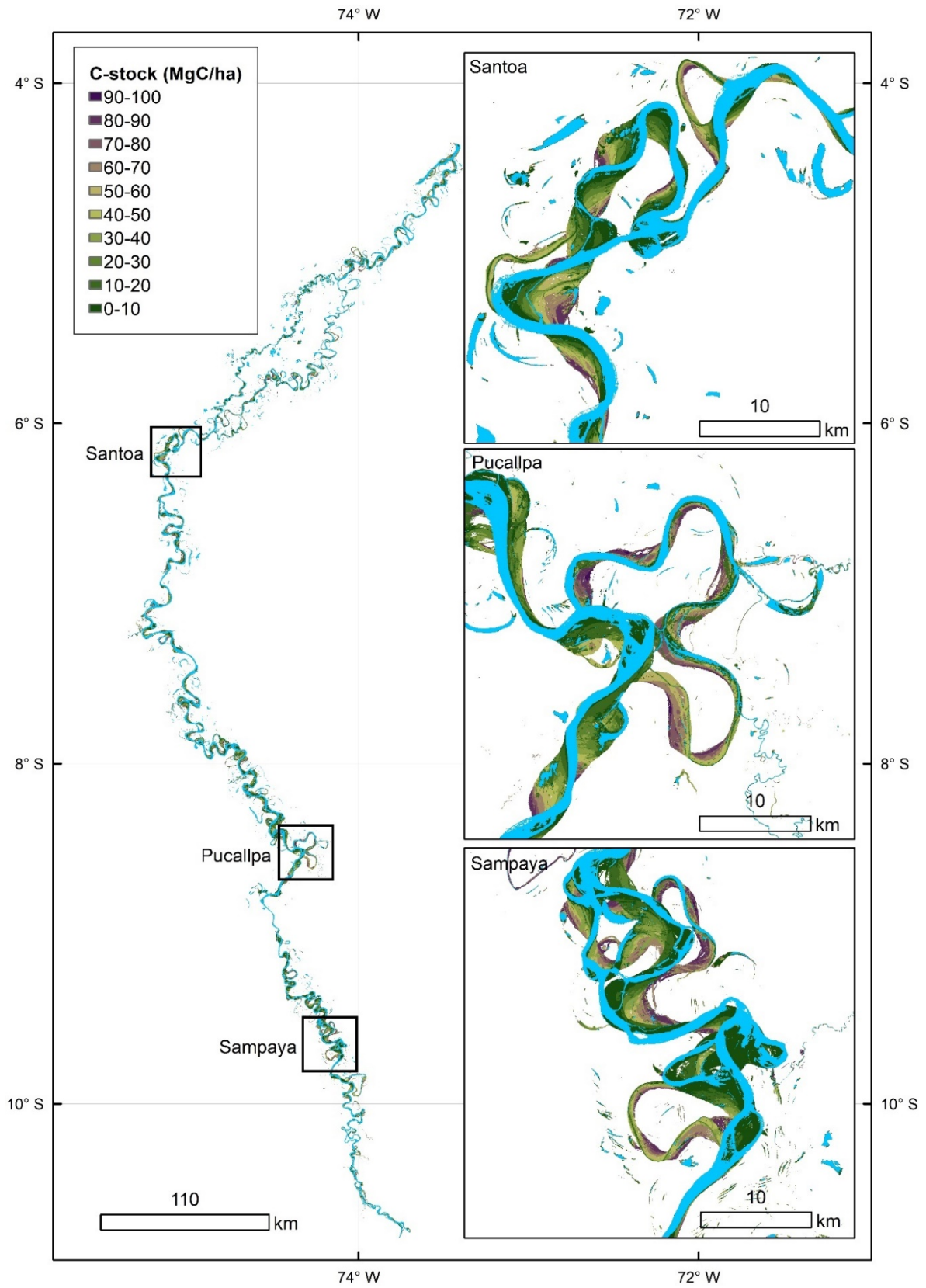
509 **Figure 6** Age structure of vegetated floodplain areas observed in the 1984-2019 active meander
510 belt. **a)** Floodplain areas according to floodplain ages established since 1984. **b)** Eroded
511 floodplain areas since 1984 according to floodplain ages. Non-determined ages (ND)
512 corresponding to floodplain or upland areas established before 1984, were considered for
513 erosion. Together, mean annual erosion accounted for $19.8 \pm 6.7 \times 10^3 \text{ ha}^{-1} \text{ yr}^{-1}$. Points and bars
514 indicate annual mean values for the period 1984-2019 and their standard deviations,
515 respectively.

516



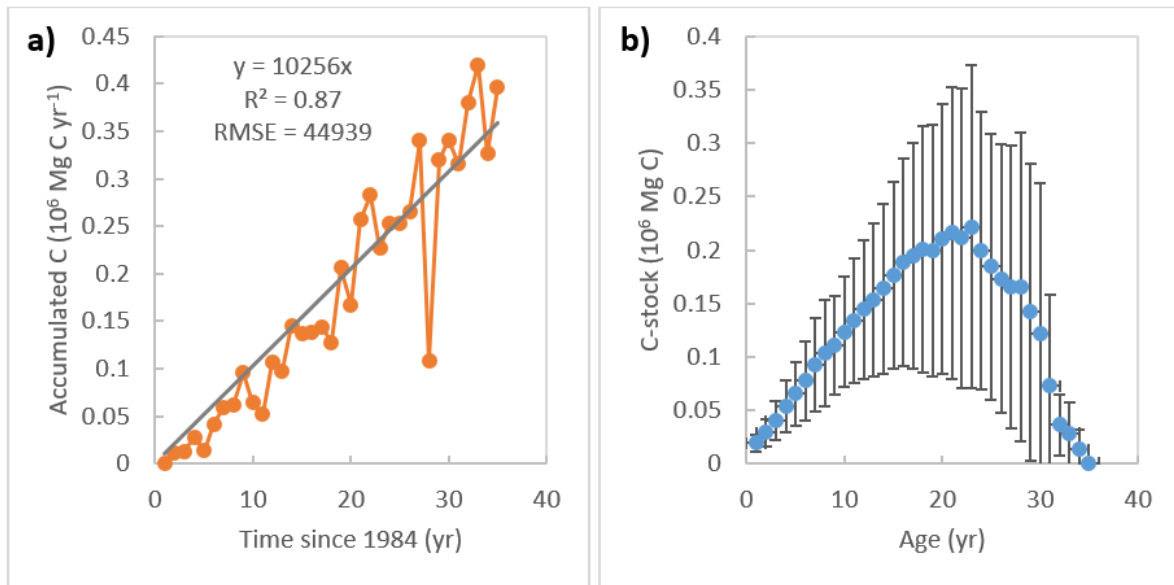
517

518 **Figure 7** Model used to derive above-ground forest C-stocks from floodplain forest age. The
519 model between 1 and 35 years (3rd polynomial; black line) is based on data (dots) published by
520 Schöngart and Wittman (2010). The data error range is $\pm 2\%$ (not indicated in the figure).
521



523
 524
 525
 526
 527

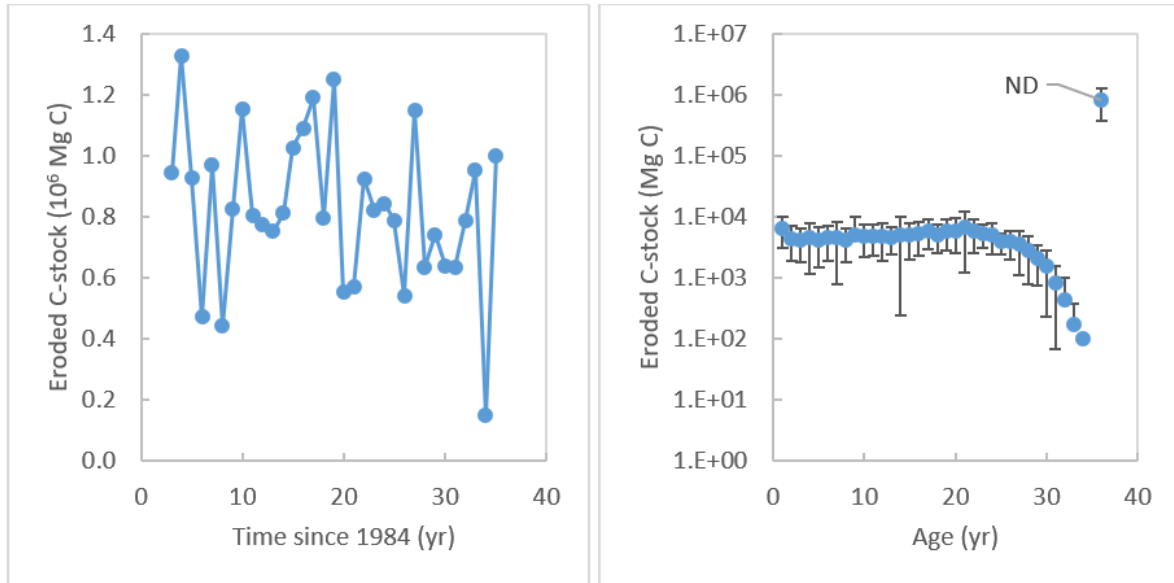
Figure 8 Above-ground floodplain forest carbon stock (C-stock in Mg C ha^{-1}) in the Ucayali 1984-2019 meander belt. Thirty yearly maps were produced for the 1984-2019 period. This figure shows the map of 2019.



528
 529
 530
 531
 532
 533
 534
 535

Figure 9 Floodplain forest carbon stocks (C-stocks) during the 1984-2019 period in the Ucayali active meander belt. **a)** Annual C accumulation in the floodplain forest established since 1984 and quantified annually until 2019. The black line indicates the annual C accumulation rate as a linear trend of 10256 Mg C yr⁻¹ ($R^2 = 0.87$, p value < 0.01 and RMSE = 44939 Mg C yr⁻¹). **b)** Annual C-stock accumulated in the floodplain forest according to the floodplain age established since 1984.

536
537



538

539 **Figure 10** Erosion of floodplain forest carbon stocks (C-stocks) caused by lateral channel
540 migration. **a)** Annual C-stocks eroded from the floodplain forest during lateral channel
541 migration between 1984 and 2019. **b)** Annual C-stock eroded from the floodplain forest during
542 lateral channel migration according to forest age. ND indicates floodplain and upland forests
543 established before 1984.
544